

# Dislocations in an arbitrary angle wedge.

## Part I: The dislocation kernel

Journal Title  
XX(X):1–7  
©The Author(s) 0000  
Reprints and permission:  
sagepub.co.uk/journalsPermissions.nav  
DOI: 10.1177/ToBeAssigned  
www.sagepub.com/

SAGE

Daniel J. Riddoch<sup>1</sup> and David A. Hills<sup>1</sup>

### Abstract

We consider the state of stress created by the presence of an edge dislocation at an arbitrary position, in a wedge of arbitrary internal angle. A method for determining the state of stress in the wedge is demonstrated and verified against finite element method simulations. Furthermore, a Mellin transform is employed to ensure that the free surfaces of the wedge remain traction free along their length.

### Keywords

dislocations, dislocation kernels, asymptotic solutions, Williams solution, complete contacts, wedge problems

### Introduction

In applied mechanics, dislocations are often used as kernels to model plastic or frictional slip or crack opening, as well as lattice defects in a crystalline structure. In this paper, we will be discussing the former. In this case, the stress caused by the dislocation, known as the kernel, is used to modify the stress present in a body under load to fulfil conditions imposed by defects, such as cracks or regions of localised slip. The stress caused by an edge dislocation in an infinite plane is well understood and concise formulae can be used to describe this stress<sup>1–3</sup>. However, no such clean formula exists for the stress resultant from a dislocation present in a semi-infinite wedge of arbitrary internal angle.

We must consider a method to determine the influence of this dislocation, starting from the solution for a dislocation in an infinite plane. The method we will use is not a new one<sup>4</sup>. We begin by reminding ourselves that the free surfaces of the wedge must be free from tractions. Now, we place a single dislocation (the object dislocation) at a given location. The stresses resulting from this dislocation can be found using the formulae for a dislocation in an infinite plane. Next, along the half-lines corresponding to the positions of the free surfaces, we place distributions of dislocations, the density of which is chosen to cancel the tractions produced by the object dislocation and ensure that the free surfaces remain traction free. This set up is shown in figure 1.

This approach was first set out by Hecker and Romanov<sup>4,5</sup> and was further considered and applied by Churchman et al<sup>6–8</sup>. All of these authors considered specific cases of the problem, and a more general form is sought. Furthermore, in order to make the analysis more practical and useable, Churchman et al truncated the interval over which the distributions of dislocations were placed, and we would like to avoid this approximation.

The object of this analysis therefore is to generalise the method in order to produce a set of solutions for any given internal wedge angle. A secondary consideration is the desire to reintroduce the Mellin transform, as described by Hecker and Romanov<sup>4</sup>, in order to increase the accuracy of the

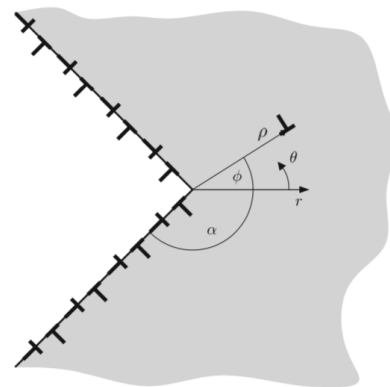


**Figure 1.** Sketch showing the method of distributing dislocations on free surfaces

solution. It should also be noted that a small error was found in the results presented by Churchman et al<sup>6</sup>, this is explained further in section and a correction is presented.

### Bilateral solution

We begin by considering the form of the state of stress in a wedge of arbitrary angle, without any dislocations present. The modelling for these stresses relies on the long established method of Williams<sup>9</sup>. The solution is an asymptotic representation of the stresses near the apex of a semi-infinite wedge. The stresses resulting are described in a polar coordinate system whose  $r$ -axis (the line  $\theta = 0$ ) is defined by the bisector line through the apex of the wedge.

<sup>1</sup>Department of Engineering Science, University of Oxford

### Corresponding author:

Daniel Riddoch, Department of Engineering Science, University of Oxford, Parks Road, OX1 3PJ Oxford, United Kingdom.

Email: daniel.riddoch@eng.ox.ac.uk

A full derivation of the representation can be found in Barber<sup>1</sup>, the upshot of which is that the stresses may generally be described by the formula

$$\sigma_{ij}(r, \theta) = K_I f_{ij}^I(\theta) r^{\lambda_I - 1} + K_{II} f_{ij}^{II}(\theta) r^{\lambda_{II} - 1} \dots \text{higher order terms.} \quad (1)$$

In this formulation  $K_I$  and  $K_{II}$  are the mode I and mode II stress intensity factors respectively,  $\lambda_I$  and  $\lambda_{II}$  are the mode 1 and mode 2 eigenvalues respectively, and  $f_{ij}^I$  and  $f_{ij}^{II}$  are the mode 1 and mode 2 eigenvectors. The method for calculating the eigenvalues and eigenvectors is detailed in .

It is known that for wedges whose total internal angle is greater than approximately  $257^\circ$ , we have that  $\lambda_I < \lambda_{II} < 1$ , and hence the contributions from both the leading eigensolutions are singular. Furthermore  $\lambda_I < \lambda_{II}$ , and for all angles greater than  $180^\circ$ , we have that  $\lambda_I < 1$ . This means that the first term in the solution will be dominant near the apex of the wedge, and is singular.

## Formulation

### Infinite plane kernels

We start with the formulae for the stress resulting from an edge dislocation. These are well known and can be found in many sources<sup>10</sup>, given in terms of Cartesian stress components and Cartesian coordinates. For a dislocation whose core is located at  $(x_d, y_d)$ , where, the resulting stress from the dislocation having Burgers vector components  $(b_x, b_y)$  is then given by

$$\sigma_{jk}(x, y, x_d, y_d) = \frac{2\mu}{\pi(\kappa + 1)} (G_{xjk}(x, y, x_d, y_d) b_x(x_d, y_d) + \dots \sigma_{\theta\theta} = \frac{\sigma_{xx} + \sigma_{yy}}{2} - \frac{\sigma_{xx} - \sigma_{yy}}{2} \cos(2\gamma) - \sigma_{xy} \sin(2\gamma) \quad (11)$$

where  $b_x$  and  $b_y$  are the Burgers vector components in the  $x$  and  $y$  directions respectively,  $\mu$  is the modulus of rigidity and  $\kappa$  is Kolosov's constant. The kernel functions  $G_{ijk}$  observed at the point  $(x, y)$  are given by

$$G_{xxx}(x, y, x_d, y_d) = -\frac{(y - y_d)(3(x - x_d)^2 + (y - y_d)^2)}{((x - x_d)^2 + (y - y_d)^2)^2} \quad (3)$$

$$G_{xxy}(x, y, x_d, y_d) = \frac{(x - x_d)((x - x_d)^2 - (y - y_d)^2)}{((x - x_d)^2 + (y - y_d)^2)^2} \quad (4)$$

$$G_{xyy}(x, y, x_d, y_d) = \frac{(y - y_d)((x - x_d)^2 - (y - y_d)^2)}{((x - x_d)^2 + (y - y_d)^2)^2} \quad (5)$$

$$G_{yxx}(x, y, x_d, y_d) = -\frac{(x - x_d)((x - x_d)^2 - (y - y_d)^2)}{((x - x_d)^2 + (y - y_d)^2)^2} \quad (6)$$

$$G_{yyx}(x, y, x_d, y_d) = \frac{(y - y_d)((x - x_d)^2 - (y - y_d)^2)}{((x - x_d)^2 + (y - y_d)^2)^2} \quad (7)$$

$$G_{yyy}(x, y, x_d, y_d) = \frac{(x - x_d)((x - x_d)^2 + 3(y - y_d)^2)}{((x - x_d)^2 + (y - y_d)^2)^2}. \quad (8)$$

We wish to use polar coordinates to formulate the problem in a robust and adaptable way. It is therefore necessary to convert these formulae to give us the stress in polar components at a location defined by polar coordinates.

This can be done in one of two ways. The most obvious method may be to rotate and transform the stress components using the coordinate transforms. Alternatively, the kernels may be derived using the Muskhelishvili potential methods. For the sake of brevity, we will discuss the first of these here only.

Firstly, let us recall the coordinate transforms. These can be derived from the definition of the coordinate systems, and are given by

$$\begin{aligned} x &= r \cos(\theta), \\ y &= r \sin(\theta). \end{aligned}$$

Next we consider the tensor transforms needed to transform the Cartesian components into polar forms. These are given by

$$\begin{aligned} \sigma_{rr} &= \frac{\sigma_{xx} + \sigma_{yy}}{2} + \frac{\sigma_{xx} - \sigma_{yy}}{2} \cos(2\gamma) + \sigma_{xy} \sin(2\gamma) \quad (9) \\ \sigma_{r\theta} &= -\frac{\sigma_{xx} - \sigma_{yy}}{2} \sin(2\gamma) + \sigma_{xy} \cos(2\gamma) \quad (10) \end{aligned}$$

where  $\gamma = \theta - \phi$ . A representation of the rotation of the state of stress is shown in figure 2.

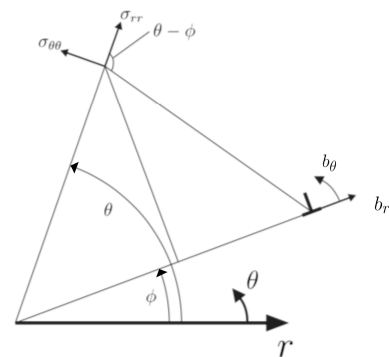


**Figure 2.** A sketch showing how the state of stress is rotated during transformation

Combining these two sets of transformations, we can now generate the kernels for the stress resulting from a dislocation

in an infinite plane in polar coordinates. These are given by

$$G_{rrr}(r, \theta, \rho, \phi) = \sin(\phi - \theta) \frac{r^3 - 2r\rho^2 - r\rho^2\cos(\phi - \theta) + 2\rho^3\cos(\phi - \theta)}{(r^2 + \rho^2 - 2r\rho\cos(\phi - \theta))^2}, \quad (12)$$

$$G_{rr\theta}(r, \theta, \rho, \phi) = \frac{r\rho(\rho\cos(3(\phi - \theta)) - 4r)}{2(r^2 + \rho^2 - 2r\rho\cos(\phi - \theta))^2} - \dots \frac{2\rho(r^2 + \rho^2)\cos(2(\phi - \theta)) + r(2r^2 + 5\rho^2)\cos(\phi - \theta)}{2(r^2 + \rho^2 - 2r\rho\cos(\phi - \theta))^2}, \quad (13)$$

$$G_{r\theta\theta}(r, \theta, \rho, \phi) = \sin(\phi - \theta) \frac{r^3 + 4r\rho^2 + r\rho^2\cos(2(\phi - \theta)) - 2\rho(2r^2 + \rho^2)\cos(\phi - \theta)}{(r^2 + \rho^2 - 2r\rho\cos(\phi - \theta))^2}, \quad (14)$$

$$G_{\theta rr}(r, \theta, \rho, \phi) = \frac{-\rho(6r^2 + 2\rho^2 + r\rho\cos(3(\phi - \theta)))}{2(r^2 + \rho^2 - 2r\rho\cos(\phi - \theta))^2} + \dots \frac{r(2r^2 + 7\rho^2)\cos(\phi - \theta)}{2(r^2 + \rho^2 - 2r\rho\cos(\phi - \theta))^2}, \quad (15)$$

$$G_{\theta r\theta}(r, \theta, \rho, \phi) = -r\sin(\phi - \theta) \frac{\rho^2\cos(2(\phi - \theta)) + r(r - 2\rho\cos(\phi - \theta))}{(r^2 + \rho^2 - 2r\rho\cos(\phi - \theta))^2}, \quad (16)$$

$$G_{\theta\theta\theta}(r, \theta, \rho, \phi) = \frac{r\rho^2\cos(3(\phi - \theta)) - 2\rho(r^2 + \rho^2)}{2(r^2 + \rho^2 - 2r\rho\cos(\phi - \theta))^2} + \dots \frac{2r^2\cos(2(\phi - \theta)) + r(2r^2 + 5\rho^2)\cos(\phi - \theta)}{2(r^2 + \rho^2 - 2r\rho\cos(\phi - \theta))^2}, \quad (17)$$

where the dislocation's core is placed at  $(\rho, \phi)$  and the stress is observed at  $(r, \theta)$ .

With these formulae now to hand, we can proceed to use them to determine the stress caused by placing a dislocation in a semi-infinite wedge of arbitrary internal angle.

### Wedge kernels formulation

Now we have the kernels for the stress in polar coordinates, we employ the same methodology described by Churchman et al.<sup>6</sup> and previously by Hecker and Romanov<sup>4,5</sup>. The approach they describe, and the one we will be using, takes the dislocation formulae just described. A single dislocation(hereafter called the object dislocation) is placed at a prescribed point in an infinite plane, and distributions of dislocations are placed along half-lines from the origin, corresponding to the free surfaces of the wedge we wish to model. The density of these dislocation distributions is then found such that the free surfaces are traction free, as required, and the combined effect of all the dislocations is now the state of stress of the object dislocation in the wedge. This concept is illustrated in Figure 1, which shows a single dislocation placed at  $(\rho, \phi)$  in a wedge of total internal angle  $2\alpha$ .

Let us now apply this method to finding the influence of a dislocation in a wedge of total internal angle  $2\alpha$ . Using the axes described by the Williams solution, we define  $\theta$  from the angle bisector, with the origin at the wedge apex. The free surfaces then fall on the two half-lines described by  $\theta = \pm\alpha$ , and  $r > 0$ . We place the dislocation at an arbitrary point with coordinates  $(\rho, \phi)$ , having that  $-\alpha < \phi < \alpha$ .

We now place continuous distributions of both glide edge and climb edge dislocations along these free surfaces, and

our object dislocation at  $(\rho, \phi)$ . This results in the formation of four simultaneous integral equations. These are detailed fully in appendix , however, they all have a similar form, so we will write explicitly only one here, viz

$$\int_0^\infty G_{rr\theta}(r, \alpha, \xi, \alpha) B_r^\oplus(\xi) + G_{\theta r\theta}(r, \alpha, \xi, \alpha) B_\theta^\oplus(\xi) + \dots G_{rr\theta}(r, \alpha, \xi, -\alpha) B_r^\ominus(\xi) + G_{\theta r\theta}(r, \alpha, \xi, -\alpha) B_\theta^\ominus(\xi) d\xi = [b_r G_{rr\theta}(r, \alpha, \rho, \phi) + b_\theta G_{\theta r\theta}(r, \alpha, \rho, \phi)], \quad (18)$$

where  $b_r$ , and  $b_\theta$  are the  $r$  direction and  $\theta$  direction components of the Burgers vector of the object dislocation, and  $B_i$  are the dislocation densities for the distributions along the free surfaces, found by

$$B_i(\xi) = \frac{db_i}{d\xi}.$$

The densities labelled  $\oplus$  correspond to distributions on the line  $\theta = \alpha$ , and those labelled  $\ominus$  with distributions along the line  $\theta = -\alpha$ . Equation 18 therefore clears the positive half-line of shear, or  $r\theta$ , tractions. The other three integral equations similarly clear both half-lines of both shear and normal tractions.

### Solving the integral equations

We now need to consider how we solve these equations. Previous studies have suggested using a Mellin transform<sup>4,5</sup>, but more recent studies have deemed a finite truncation of the integral range to be sufficient<sup>6</sup>. We will now use a standard inversion method of the Gauss-Chebyshev type. The method behind this inversion is described by Hills et al<sup>10</sup>, and we will now describe our application of this method.

First, we must ensure that we are right to apply this method. As described in section , the stresses in the wedge without the dislocation present are singular at the wedge apex, of the order  $r^{\lambda_I-1}$ . For the sake of convenience, we may simply treat this as square root singular. Previous studies<sup>6,11</sup> considering similar problems indicate that this does not affect convergence. Away from the apex, the stress decreases monotonically, and so we must choose a fundamental function that is singular at one end, and bounded at the other.

We can therefore transform the radial coordinates in order to change the integration range to the interval  $[-1, 1]$  in order to use the quadrature. We introduce a transform for the collocation(observation) points

$$r = \frac{l \log\left(\frac{2}{1+t}\right)}{2 \log 2}, \quad (19)$$

and a similar transform for the integration points

$$\xi = \frac{l \log\left(\frac{2}{1+s}\right)}{2 \log 2}, \quad (20)$$

where  $l$  is an arbitrary multiplier. Hence, we choose as the fundamental function the function  $\omega(s_j)$  having the form

$$\omega(s) = \sqrt{\frac{1-s}{1+s}}, \quad (21)$$

and so we now rewrite the dislocation densities in the form

$$B_i(\xi) = \omega(\xi)\varphi_i(\xi). \quad (22)$$

Now, the numerical quadrature, as described by Erdogan et al<sup>12</sup> for the choice of fundamental function, as in equation 21, leads to the following formulations for the integration and collocation points

$$t = \cos\left(\frac{\pi(2i-1)}{2n+1}\right) \quad (23)$$

$$s = \cos\left(\frac{2i\pi}{2n+1}\right), \quad (24)$$

for some predetermined number of points  $n$ , where  $i = 1, \dots, n$ . Finally, we introduce the weighting function

$$W(s) = \frac{2(1-s)}{2n+1}, \quad (25)$$

which allows us to discretise the integral equation.

Equation 18 therefore can first be rewritten as

$$\begin{aligned} \int_{-1}^1 \left( G_{rr\theta} \left( \frac{l}{2} \frac{\log \frac{2}{1+t}}{\log 2}, \alpha, \frac{l}{2} \frac{\log \frac{2}{1+s}}{\log 2}, \alpha \right) B_r^\oplus(s) + \dots \right. \\ G_{\theta r\theta} \left( \frac{l}{2} \frac{\log \frac{2}{1+t}}{\log 2}, \alpha, \frac{l}{2} \frac{\log \frac{2}{1+s}}{\log 2}, \alpha \right) B_\theta^\oplus(s) + \dots \\ G_{rr\theta} \left( \frac{l}{2} \frac{\log \frac{2}{1+t}}{\log 2}, \alpha, \frac{l}{2} \frac{\log \frac{2}{1+s}}{\log 2}, -\alpha \right) B_r^\ominus(s) + \dots \\ \left. G_{\theta r\theta} \left( \frac{l}{2} \frac{\log \frac{2}{1+t}}{\log 2}, \alpha, \frac{l}{2} \frac{\log \frac{2}{1+s}}{\log 2}, -\alpha \right) B_\theta^\ominus(s) \right) \\ \frac{l}{2(s+1)\log 2} ds = \left[ b_r G_{rr\theta} \left( \frac{l}{2} \frac{\log \frac{2}{1+t}}{\log 2}, \alpha, \rho, \phi \right) + \dots \right. \\ \left. b_\theta G_{\theta r\theta} \left( \frac{l}{2} \frac{\log \frac{2}{1+t}}{\log 2}, \alpha, \rho, \phi \right) \right], \quad (26) \end{aligned}$$

by applying the transforms. Notice that generally we find  $G_{ijk}(\gamma r, \alpha, \gamma \rho, \phi) = \frac{1}{\gamma} G_{ijk}(r, \alpha, \rho, \phi)$ , so the IE becomes

$$\begin{aligned} \int_{-1}^1 \left( G_{rr\theta} \left( \log \frac{2}{1+t}, \alpha, \log \frac{2}{1+s}, \alpha \right) B_r^\oplus(s) + \dots \right. \\ G_{\theta r\theta} \left( \log \frac{2}{1+t}, \alpha, \log \frac{2}{1+s}, \alpha \right) B_\theta^\oplus(s) + \dots \\ G_{rr\theta} \left( \log \frac{2}{1+t}, \alpha, \log \frac{2}{1+s}, -\alpha \right) B_r^\ominus(s) + \dots \\ \left. G_{\theta r\theta} \left( \log \frac{2}{1+t}, \alpha, \log \frac{2}{1+s}, -\alpha \right) B_\theta^\ominus(s) \right) \frac{1}{s+1} ds \\ = \left[ b_r G_{rr\theta} \left( \frac{l}{2} \frac{\log \frac{2}{1+t}}{\log 2}, \alpha, \rho, \phi \right) + \dots \right. \\ \left. b_\theta G_{\theta r\theta} \left( \frac{l}{2} \frac{\log \frac{2}{1+t}}{\log 2}, \alpha, \rho, \phi \right) \right]. \quad (27) \end{aligned}$$

Finally, rewriting the dislocation densities, we find,

$$\begin{aligned} \sum_{i=1}^n \left( G_{rr\theta} \left( \log \frac{2}{1+t}, \alpha, \log \frac{2}{1+s(i)}, \alpha \right) \varphi_r^\oplus(s(i)) W(s(i)) + \dots \right. \\ G_{\theta r\theta} \left( \log \frac{2}{1+t}, \alpha, \log \frac{2}{1+s(i)}, \alpha \right) \varphi_\theta^\oplus(s(i)) W(s(i)) + \dots \\ G_{rr\theta} \left( \log \frac{2}{1+t}, \alpha, \log \frac{2}{1+s(i)}, -\alpha \right) \varphi_r^\ominus(s(i)) W(s(i)) + \dots \\ \left. G_{\theta r\theta} \left( \log \frac{2}{1+t}, \alpha, \log \frac{2}{1+s(i)}, -\alpha \right) \varphi_\theta^\ominus(s(i)) W(s(i)) \right) \\ \frac{1}{s(i)+1} = \left[ b_r G_{rr\theta} \left( \frac{l}{2} \frac{\log \frac{2}{1+t}}{\log 2}, \alpha, \rho, \phi \right) + \dots \right. \\ \left. b_\theta G_{\theta r\theta} \left( \frac{l}{2} \frac{\log \frac{2}{1+t}}{\log 2}, \alpha, \rho, \phi \right) \right]. \quad (28) \end{aligned}$$

We have shown how to discretise one of the equations, and the other three follow suit. These four equations then produce  $4n$  equations, in  $4n$  unknowns. These are the values of the functions denoted

$$\begin{aligned} \varphi_r^\oplus(s_1), \dots, \varphi_r^\oplus(s_n), \varphi_r^\ominus(s_1), \dots, \varphi_r^\ominus(s_n), \varphi_\theta^\oplus(s_1), \dots \\ \varphi_\theta^\oplus(s_n), \varphi_\theta^\ominus(s_1), \dots, \varphi_\theta^\ominus(s_n). \quad (29) \end{aligned}$$

## Results and verification

The solutions to the equations above allow us to distribute dislocations along the free surfaces, to ensure that they remain traction free while the influence of the object dislocation is also felt throughout the wedge. It is important to note that for  $|r - \rho| \ll 1$ , ie close to the core of the object dislocation, the singularity induced by the dislocation will be dominant, but otherwise, the free surfaces will have a greater impact on the local state of stress. As such, when representing the solution, it makes sense to split the solution for the kernel into two parts. The influence of the object dislocation is given by  $G_{ijk}$ , and the influence of the free surfaces is denoted by  $F_{ijk}$ .

Thus far, in the formulation and the method we have, very deliberately, maintained total generality of the wedge angle, and the dislocation location. We have therefore, the ability to find the kernel for any given position of the object dislocation, and any given wedge angle. Now, however, we must specify these angles and locations in order to display the results.

### The three-quarter plane

Firstly, let us consider the three-quarter plane, or 270 degree wedge. The case of the three-quarter plane, with the object dislocation at the angle  $\phi = \frac{\pi}{4}$  has been extensively considered before by Churchman et al<sup>6</sup>.

Whilst their method has generally been followed, a Mellin transform has been employed. This should improve the accuracy. It should also be noted that we have taken pains not to normalise the distances along the free surfaces from the wedge apex by the distance of the object dislocation from the apex. One of the assumptions of this normalisation is that  $F_{ijk}(r, \theta, \rho, \phi) = F_{ijk}(\gamma r, \theta, \gamma \rho, \phi)$ , where  $F_{ijk}$  are the influence functions defined above. This argument does

not strictly hold. It is accurate to say that  $\bar{\sigma}_{jk}(r, \theta, \rho, \phi) = \bar{\sigma}_{jk}(\gamma r, \theta, \gamma \rho, \phi)$ , where  $\gamma$  is some real number and  $\bar{\sigma}_{jk}(\gamma r, \theta, \gamma \rho, \phi) = \gamma b_i F_{ijk}(\gamma r, \theta, \gamma \rho, \phi)$ . Therefore

$$\begin{aligned} \gamma b_i F_{ijk}(\gamma r, \theta, \gamma \rho, \phi) &= b_i F_{ijk}(r, \theta, \rho, \phi), \\ F_{ijk}(\gamma r, \theta, \gamma \rho, \phi) &= \frac{1}{\gamma} F_{ijk}(r, \theta, \rho, \phi). \end{aligned} \quad (30)$$

Now we may consider and compare the results from our method, to those found by Churchman et al. Figure 3 shows plot of all four relevant  $F_{ijk}$  functions, with our results shown in blue(solid line), and Churchman's results overlaid in red(dotted line). We can see from this figure that our results match almost perfectly.

As discussed by Churchman, it is possible to fit a function to these influence functions. However, we will not replicate that here. The reasons for not doing so are two-fold. Firstly, we will display many different new results for many different angles, reproducing sufficient coefficients for all the relevant fits would impractical. Secondly, as part of this publication, we are publishing the MATLAB code used to produce these curves. As such, the reader may use this code to reproduce these curves exactly; the added error which will inevitably be introduced by a fit can then be avoided.

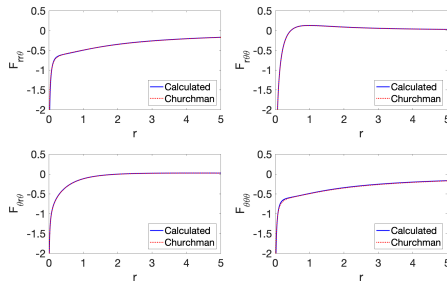


**Figure 3.** Overlay plots comparing our results to those of Churchman<sup>6</sup>.

### The half-plane

The problem of the influence of a dislocation in a half-plane has a closed form solution. It is described by Hills et al<sup>10</sup>. Our solution may again be repurposed to compare these kernels. Figure 4 shows an overlay of our results for the kernels of a dislocation at a position of unit distance perpendicular to the free surface, observed along a line, also perpendicular to the surface, running through the dislocation core.

As before, our results are shown in blue(solid line) and the results of Hills et al are shown overlaid in red(dotted line). Once again, inspection of the figure shows that our results are near identical to those calculated analytically.

### The continuation line

There are many more combinations of angles that may be considered. Our results may, for example, be compared to those of Philipps et al<sup>13</sup>. However, we will content ourselves here by considering the case of a dislocation placed on the continuation line of one of the free surfaces in a wedge of varying angle, the continuation line being a half-line

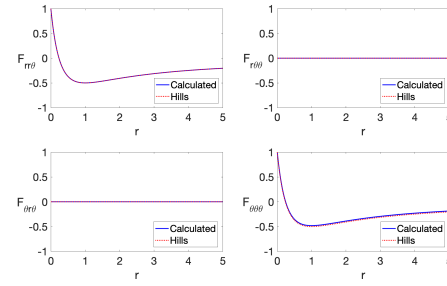


**Figure 4.** Overlay plots comparing our results to those calculated from Hills et al<sup>10</sup>.

collinear to one of the free surfaces originating from the notch apex.

This time, a finite element analysis has been conducted to verify our findings. Again the results are plotted with our results shown in blue(solid line) and the FE data shown in red(dotted line). Several different wedge angles are considered, and these results are plotted in Figures 5, 6, 7, for total internal wedge angles of 240°, 280° and 340°. Comparisons have been made with 44 different angle values using FEM, and the FEM data is published along with the code generating the curves, so the reader may inspect all of these comparisons. For the sake of brevity, we only reproduce three such figures here.

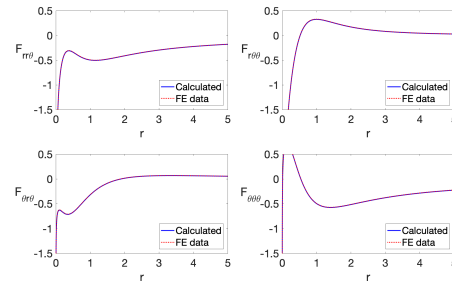


**Figure 5.** Overlay plots comparing our results to and FEM analysis at an internal wedge angle of 240°.

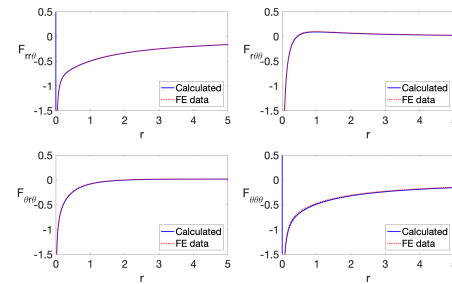


**Figure 6.** Overlay plots comparing our results to and FEM analysis at an internal wedge angle of 280°.

An inspection of these figures once again shows that our results almost exactly match the FE solution. It is worth noting in some cases numerical problems related to singularities may cause errors in the two or three points closest to the wedge apex. This is simply a numerical feature caused by the interaction of many singularities very close to

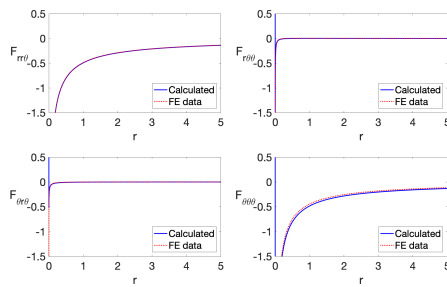


**Figure 7.** Overlay plots comparing our results to and FEM analysis at an internal wedge angle of  $340^\circ$ .

the wedge apex, and does not reflect any inaccuracies within the method or the results outside of this very small area.

## Conclusion

This analysis has derived a general method for finding the influence of an edge dislocation in a semi-infinite wedge of arbitrary internal angle. This has been done using the more accurate Mellin transform method, and the use of polar coordinates has allowed the problem to be generalised for an arbitrary internal angle.

The solution has been verified by comparison with known results and finite element analysis. In all cases the singularity caused by the dislocation has been considered separately to the influence of the free surfaces. The influence functions produced can now be used to consider the behaviour of cracks and/or slip regions near the edge of a complete contact. MATLAB code providing a transportable, verified form of the solutions for incorporation into numerical analysis of cracks, slip zones etc is available with this document as supplementary files.

## Acknowledgements

Both authors thank Rolls-Royce plc and the EPSRC for the support under the Prosperity Partnership Grant 'Cornerstone: Mechanical Engineering Science to Enable Aero Propulsion Futures', Grant Ref: EP/R004951/1.

## References

1. Barber JR. *Elasticity*. Springer, 2010.
2. Barber J. *Contact Mechanics*. Springer, 2018.
3. Johnson KL. *Contact mechanics*. Cambridge university press, 1987.
4. Hecker M and Romanov A. The stress fields of an edge dislocation near a wedge-shaped boundary. *physica status solidi (a)* 1992; 130(1): 91–101.
5. Hecker M and Romanov A. The stress fields of edge dislocations near wedge-shaped boundaries and bonded wedges. In *Fundamental Aspects of Dislocation Interactions*. Elsevier, 1993. pp. 411–414.
6. Churchman C, Korsunsky A and Hills D. The edge dislocation in a three-quarter plane. part i: Influence functions. *European Journal of Mechanics-A/Solids* 2006; 25(1): 42–50.
7. Churchman C and Hills D. The edge dislocation in a three-quarter plane. part ii: Application to an edge crack. *European Journal of Mechanics-A/Solids* 2006; 25(3): 389–396.
8. Churchman C and Hills D. Slip zone length at the edge of a complete contact. *International Journal of Solids and structures* 2006; 43(7-8): 2037–2049.
9. Williams M. Stress singularities resulting from various boundary conditions in angular corners of plates in extension. *Journal of applied mechanics* 1952; 19(4): 526–528.
10. Hills DA, Kelly PA, Dai DN et al. *Solution of crack problems: the distributed dislocation technique*, volume 44. Springer Science & Business Media, 2013.
11. Yingzhi L and Hills D. Stress intensity factor solutions for kinked surface cracks. *The Journal of Strain Analysis for Engineering Design* 1990; 25(1): 21–27.
12. Erdogan F, Gupta GD and Cook T. Numerical solution of singular integral equations. In *Methods of analysis and solutions of crack problems*. Springer, 1973. pp. 368–425.
13. Philipps A, Karuppanan S, Churchman C et al. Crack tip stress intensity factors for a crack emanating from a sharp notch. *Engineering Fracture Mechanics* 2008; 75(18): 5134–5139.

## Williams solution

A brief description of the Williams solution is given in section . In this appendix we outline the method of finding the eigenvalues and eigenvectors.

Firstly, let us calculate the eigenvalues, these are the solution of the characteristic equations

$$\lambda_I \sin(2\alpha) + \sin(2\alpha\lambda_I) = 0 \quad \& \quad \lambda_{II} \sin(2\alpha) - \sin(2\alpha\lambda_{II}) = 0. \quad (31)$$

In order to avoid trivial solutions and ensure the appropriate singular behaviour, we must enforce constraints on the eigenvalues. Both eigenvalues must be positive, and  $\lambda_{II} > \lambda_I$ , except in the special case  $\phi = \pi$ , in which case we find  $\lambda_I = \lambda_{II} = 0.5$ . Finally  $\lambda_I \neq 1$  and  $\lambda_{II} \neq 1$  as these are trivial solutions.

The corresponding eigenvectors are found by

$$f_{rr}^I(\psi) = \frac{\cos[(\lambda_I - 1)\alpha]\cos[(\lambda_I + 1)\psi] - \frac{\lambda_I - 3}{\lambda_I + 1}\cos[(\lambda_I + 1)\alpha]\cos[(\lambda_I - 1)\psi]}{\cos[(\lambda_I + 1)\alpha] - \cos[(\lambda_I - 1)\alpha]} \quad (32)$$

$$f_{rr}^{II}(\psi) = \frac{\sin[(\lambda_{II} - 1)\alpha]\sin[(\lambda_{II} + 1)\psi] - \frac{\lambda_{II} - 3}{\lambda_{II} + 1}\sin[(\lambda_{II} + 1)\alpha]\sin[(\lambda_{II} - 1)\psi]}{\sin[(\lambda_{II} - 1)\alpha] - \frac{\lambda_{II} - 1}{\lambda_{II} + 1}\sin[(\lambda_{II} + 1)\alpha]} \quad (33)$$

$$f_{r\theta}^I(\psi) = \frac{\sin[(\lambda_I - 1)\alpha]\sin[(\lambda_I + 1)\psi] - \sin[(\lambda_I + 1)\alpha]\sin[(\lambda_I - 1)\psi]}{\sin[(\lambda_I - 1)\alpha] - \frac{\lambda_I + 1}{\lambda_I - 1}\sin[(\lambda_I + 1)\alpha]} \quad (34)$$

$$f_{r\theta}^{II}(\psi) = \frac{\cos[(\lambda_{II} - 1)\alpha]\cos[(\lambda_{II} + 1)\psi] - \cos[(\lambda_{II} + 1)\alpha]\cos[(\lambda_{II} - 1)\psi]}{\cos[(\lambda_{II} - 1)\alpha] - \cos[(\lambda_{II} + 1)\alpha]} \quad (35)$$

$$f_{\theta\theta}^I(\psi) = \frac{\cos[(\lambda_I - 1)\alpha]\cos[(\lambda_I + 1)\psi] - \cos[(\lambda_I + 1)\alpha]\cos[(\lambda_I - 1)\psi]}{\cos[(\lambda_I - 1)\alpha] - \cos[(\lambda_I + 1)\alpha]} \quad (36)$$

$$f_{\theta\theta}^{II}(\psi) = \frac{\sin[(\lambda_{II} - 1)\alpha]\sin[(\lambda_{II} + 1)\psi] - \sin[(\lambda_{II} + 1)\alpha]\sin[(\lambda_{II} - 1)\psi]}{-\sin[(\lambda_{II} - 1)\alpha] + \frac{\lambda_{II} - 1}{\lambda_{II} + 1}\sin[(\lambda_{II} + 1)\alpha]} \quad (37)$$

## Integral equations

$$\begin{aligned} \int_0^\infty G_{rr\theta}(r, \alpha, \xi, \alpha) B_r^\oplus(\xi) + G_{\theta r\theta}(r, \alpha, \xi, \alpha) B_\theta^\oplus(\xi) + G_{rr\theta}(r, \alpha, \xi, -\alpha) B_r^\ominus(\xi) + G_{\theta r\theta}(r, \alpha, \xi, -\alpha) B_\theta^\ominus(\xi) d\xi \\ = [b_r G_{rr\theta}(r, \alpha, \rho, \phi) + b_\theta G_{\theta r\theta}(r, \alpha, \rho, \phi)] \end{aligned} \quad (38)$$

$$\begin{aligned} \int_0^\infty G_{rr\theta}(r, -\alpha, \xi, \alpha) B_r^\oplus(\xi) + G_{\theta r\theta}(r, -\alpha, \xi, \alpha) B_\theta^\oplus(\xi) + G_{rr\theta}(r, -\alpha, \xi, -\alpha) B_r^\ominus(\xi) + G_{\theta r\theta}(r, -\alpha, \xi, -\alpha) B_\theta^\ominus(\xi) d\xi \\ = [b_r G_{rr\theta}(r, -\alpha, \rho, \phi) + b_\theta G_{\theta r\theta}(r, -\alpha, \rho, \phi)] \end{aligned} \quad (39)$$

$$\begin{aligned} \int_0^\infty G_{r\theta\theta}(r, \alpha, \xi, \alpha) B_r^\oplus(\xi) + G_{\theta\theta\theta}(r, \alpha, \xi, \alpha) B_\theta^\oplus(\xi) + G_{r\theta\theta}(r, \alpha, \xi, -\alpha) B_r^\ominus(\xi) + G_{\theta\theta\theta}(r, \alpha, \xi, -\alpha) B_\theta^\ominus(\xi) d\xi \\ = [b_r G_{r\theta\theta}(r, \alpha, \rho, \phi) + b_\theta G_{\theta\theta\theta}(r, \alpha, \rho, \phi)] \end{aligned} \quad (40)$$

$$\begin{aligned} \int_0^\infty G_{r\theta\theta}(r, -\alpha, \xi, \alpha) B_r^\oplus(\xi) + G_{\theta\theta\theta}(r, -\alpha, \xi, \alpha) B_\theta^\oplus(\xi) + G_{r\theta\theta}(r, -\alpha, \xi, -\alpha) B_r^\ominus(\xi) + G_{\theta\theta\theta}(r, -\alpha, \xi, -\alpha) B_\theta^\ominus(\xi) d\xi \\ = [b_r G_{r\theta\theta}(r, -\alpha, \rho, \phi) + b_\theta G_{\theta\theta\theta}(r, -\alpha, \rho, \phi)] \end{aligned} \quad (41)$$